TIFR/TH/00-04

IMSc/2000/01/02

hep-ph/0001287

A QCD Analysis of Polarised Parton Densities

Dilip Kumar Ghosh and Sourendu Gupta

Department of Theoretical Physics,
Tata Institute of Fundamental Research,
Homi Bhabha Road, Bombay 400005, India.

D. Indumathi

The Institute of Mathematical Sciences,
CIT Campus, Chennai 600113, India.

Abstract

We present the results of a QCD fit to global data on deep-inelastic polarised lepton-hadron scattering. We find that it is possible to fit the data with strongly broken $SU(2)$ flavour for the polarised sea densities. This can easily be tested in W production at polarised RHIC. The data fails to pin down polarised singlet sea quark and gluon densities. We explore the uncertainties in detail and show that improvement in statistics, achievable at polarised HERA for measurement of A_1 at moderately low values of x, have large payoffs in terms of the improvement in measurement of gluon and sea quark densities.

1 Introduction

It is now more than a decade since the first polarised DIS experiments [1] discovered the strong breaking of a $SU(6)$ quark model based sum-rule [2], and precipitated the "proton spin crisis". Since then many polarised deep-inelastic scattering (DIS) experiments have reported measurements of the virtual photon asymmetry

$$A_1(x,Q^2) = \frac{g_1(x,Q^2)}{F_1(x,Q^2)} \tag{1}$$

on different targets (the structure functions g_1 and F_1 are defined later). A polarised proton collider at RHIC will soon begin to constrain the unknown polarised parton distributions even more strongly. Current and future interest in this topic stems partly from the history of the "spin crisis".

However, polarised parton densities are also interesting because of the role they might play in future polarised hadron collider searches for completions of the standard model. Essentially, a large variety of physics beyond the standard model plays with chirality. Some of this freedom can easily be curtailed by polarised scattering experiments, if the polarised parton densities are known with precision. We expect that by the end of the polarised-RHIC program this goal should be reached.

The longitudinally polarised structure function g_1 is defined by

$$g_1(x,Q^2) = \widetilde{\mathcal{C}}_q \otimes \frac{1}{2}\sum_f e_f^2 \left[\widetilde{q}_f + \widetilde{\bar{q}}_f\right] + \frac{1}{2}\left(\sum_f e_f^2\right)\widetilde{\mathcal{C}}_g \otimes \widetilde{g}, \tag{2}$$

which is a Mellin convolution of the quark ($\widetilde{q}_f$), anti-quark ($\widetilde{\bar{q}}_f$) and gluon ($\widetilde{g}$) longitudinally polarised distributions with the coefficient functions $\widetilde{\mathcal{C}}_{q,g}$. The index f denotes flavour, and e_f is the charge carried by the quark. The unpolarised structure function is given by a similar formula in terms of the corresponding unpolarised densities and coefficient functions.

These coefficient functions and the splitting functions (which determine the evolution of the densities) are computable order by order in perturbative QCD. The former are crucial for the Bjorken sum rule [3], connecting the proton and neutron structure functions, g_1^p and g_1^n, to the neutron β-decay constant g_A, and are known to NNLO [4]. This makes it possible to use

this sum rule for precision measurement of the QCD scale [5]. The polarised splitting functions are known only at NLO [6].

In this paper we analyse the currently available inclusive DIS data in QCD and extract polarised parton distributions from them. In this respect our work is similar to that of [7]. However, our analysis differs in several ways. For one, some of the data we use is more recent than the older fits. More importantly, we relax some of the assumptions which needed to be made in analysing the older data. We allow for flavour asymmetry in the polarised sea quark densities, and let the first moment of the gluon density vary freely in the fit. Furthermore we make a detailed investigation of the uncertainties in these polarised gluon and sea quark densities.

The uncertainty in gluon densities may seem puzzling in view of the fact that the Q^2-dependence of the structure function g_1 involves the gluon strongly. In fact, at LO we already have—

$$\frac{\partial g_1}{\partial \log Q^2} = \frac{\alpha_s}{2\pi}\left[\widetilde{P}_{qq} \otimes g_1 + \widetilde{P}_{qg} \otimes \widetilde{g}\right], \tag{3}$$

where $\widetilde{P}_{qq}$ and $\widetilde{P}_{qg}$ are polarised splitting functions. Since α_s is now very strongly constrained by measurements at LEP and through unpolarised DIS, one might expect that data on g_1 constrains the polarised gluon densities. Unfortunately, errors on g_1 are large in the low-x region, where the contribution of the gluons dominate, primarily because the asymmetry A_1 is small at low-x. For the same reason the flavour singlet sea quark density is also rather loosely constrained by data. We investigate the statistics necessary to improve these constraints through DIS measurements of A_1 at polarised HERA.

The plan of this paper is the following. In the next section we discuss the various technicalities that distinguish different global analyses. This section also serves to set up the notation. This is followed by a section that discusses our choice of data used in the fit. The next section contains our results for the LO and NLO fits, and a detailed consideration of the parameter errors. A section on some applications of our parametrisations follows this. The final section contains a summary of our main results.

2 Constraints on parton densities

2.1 Parton densities and structure functions

With N_f flavours of quarks, we need to fix $2N_f + 1$ parton densities. These are for the $2N_f$ flavours of quarks and anti-quarks and the gluon. For protons or neutrons, the quark and anti-quark densities for the strange and heavier flavours are equal. We work with the two (flavour non-singlet) polarised valence quark densities, $\widetilde{V}_u$ and $\widetilde{V}_d$, corresponding to the up and down flavours. The other non-singlet densities we use are those corresponding to the diagonal generators of $SU(5)$ flavour—

$$\begin{aligned} \widetilde{q}_3 &\equiv 2(\widetilde{\bar{u}} - \widetilde{\bar{d}}), \qquad \widetilde{q}_8 \equiv 2(\widetilde{\bar{u}} + \widetilde{\bar{d}} - 2\widetilde{\bar{s}}), \\ \widetilde{q}_{15} &\equiv 2(\widetilde{\bar{u}} + \widetilde{\bar{d}} + \widetilde{\bar{s}} - 3\widetilde{\bar{c}}), \qquad \widetilde{q}_{24} \equiv 2(\widetilde{\bar{u}} + \widetilde{\bar{d}} + \widetilde{\bar{s}} + \widetilde{\bar{c}} - 4\widetilde{\bar{b}}). \end{aligned} \tag{4}$$

The initial conditions for evolution are that below and at each flavour threshold, the density for that flavour of quarks is zero. Thus, below the charm threshold we have $\widetilde{q}_{24} = \widetilde{q}_{15} = \widetilde{q}_0$ and below the bottom threshold we set $\widetilde{q}_{24} = \widetilde{q}_0$. For the singlet quark density, we use

$$\widetilde{q}_0 \equiv 2\sum_f \widetilde{\bar{q}}_f = \widetilde{\Sigma} - \sum_f \widetilde{V}_f, \tag{5}$$

in preference to the usual $\widetilde{\Sigma}$ (which is the sum over quark and anti-quark densities of all flavours). The evolution equations couple $\widetilde{q}_0$ to the gluon density $\widetilde{g}$. We also define similar unpolarised quark and gluon densities[1].

Finally, the structure function g_1^p, for the proton, is given by

$$\begin{aligned} &g_1^p(x,Q^2) = \widetilde{\mathcal{C}}_q \otimes \widetilde{h} + \widetilde{\mathcal{C}}_g \otimes \widetilde{g}, \qquad \text{where} \\ &\widetilde{h} = \frac{1}{18}\left[4\widetilde{V}_u + \widetilde{V}_d + \frac{22}{10}\widetilde{q}_0 + \frac{3}{2}\widetilde{q}_3 + \frac{1}{2}\widetilde{q}_8 - \frac{1}{2}\widetilde{q}_{15} + \frac{3}{10}\widetilde{q}_{24}\right]. \end{aligned} \tag{6}$$

The unpolarised structure function F_1^p is also given by a similar expression. The structure functions for the neutron, g_1^n, are obtained by an isospin flip—interchanging $\widetilde{V}_u$ and $\widetilde{V}_d$ and switching the sign of $\widetilde{q}_3$. After correcting for

[1] Our convention is that polarised quantities are distinguished from the corresponding unpolarised ones by a tilde.

nuclear effects, the normalised structure function for deuterium is $g_1^d = (g_1^p + g_1^n)/2$, and a similar expression for F_1^d.

We shall have occasion to use the first moments of various polarised parton distributions. We introduce the notation—

$$\Gamma_u(Q^2) = \int_0^1 dx\, \widetilde{V}_u(x,Q^2), \qquad \Gamma_d(Q^2) = \int_0^1 dx\, \widetilde{V}_d(x,Q^2),$$

$$\Gamma_i(Q^2) = \int_0^1 dx\, \widetilde{q}_i(x,Q^2), \qquad \Gamma_g(Q^2) = \int_0^1 dx\, \widetilde{g}(x,Q^2). \tag{7}$$

(8)

We will also use the notation $\Gamma_V^0 = \Gamma_u + \Gamma_d$ and $\Gamma_V^3 = \Gamma_u - \Gamma_d$. The notation

$$\Gamma_1^{n,p}(Q^2) = \int_0^1 dx\, g_1^{n,p}(x,Q^2) \tag{9}$$

is fairly standard. We shall use it in the text. We also use the notation $\Gamma_{\bar{u}}$, *etc.*, to denote the first moments of the flavoured sea densities.

2.2 The fitting strategy

We use experimental data on the asymmetries A_1^p, A_1^n and A_1^d, measured on proton, neutron (He^3) and deuterium targets to constrain the polarised parton densities. We assume full knowledge of the unpolarised parton densities as given by some global fit, so that the structure function F_1 can be reconstructed using appropriate NLO coefficient functions. Then the data on A_1 can be converted to g_1. We prefer this method to taking the g_1 values presented by experiments, since different experimental groups may make different assumptions about the unpolarised structure functions. Such effects would lead to additional normalisation uncertainties in any global fit.

We have chosen to use the CTEQ4 set of parton densities [8] in our work. We do not expect this choice to affect our conclusions strongly since the unpolarised parton densities now have smaller errors than data on the polarisation asymmetry A_1. However, with this choice we are constrained to follow some of the assumptions made by the CTEQ group—

1. We work in the $\overline{\rm MS}$ scheme, since the CTEQ group does that. Other possibilities would have been to work in the AB [9] or JET [10] schemes, but then we would have had to transform the CTEQ distributions. We

prefer to avoid this procedure, since the best fit parton densities in one scheme do not necessarily transform into the best fit densities in another scheme.

2. We retain the CTEQ choice for the charm quark mass being 1.6 GeV and the bottom quark mass to be 5.0 GeV. At each mass threshold, we increase the number of flavours by one, and treat the newly activated flavour as massless immediately above the threshold. Parton distributions and α_s are continuous across these thresholds [11].

3. We are constrained to use the Λ_{QCD} values used in [8].

4. We take $Q_0^2 = 2.56$ GeV^2 in order to avoid having to evolve the unpolarised parton densities downwards.

In future we plan to study the results of relaxing one or more of these restrictions.

We follow the parametrisation of CTEQ4 and write—

$$\widetilde{f}(x, Q_0^2) = a_0 x^{a_1}(1-x)^{a_2}(1 + a_3 x^{a_4}), \tag{10}$$

for all densities apart from q_3, which is parametrised as

$$\widetilde{q}_3(x, Q_0^2) = a_0 x^{a_1}(1-x)^{a_2}(1 + a_3\sqrt{x} + a_4 x). \tag{11}$$

We have made the choice that the large-x behaviour of any polarised density is the same as that of the unpolarised density; in other words, the parameter a_2 is the same for corresponding polarised and unpolarised densities (this assumption is sometimes given the name "helicity retention property" [12]). For simplicity we have also equated the polarised and unpolarised values of a_4 when this parameter is a power.

Finally, at Q_0^2 we have extended some of the CTEQ assumptions for unpolarised parton densities to polarised. These include equating the values of a_1 for $\widetilde{V}_u$, $\widetilde{V}_d$ and $\widetilde{q}_3$, taking $a_4 = 1$ for $\widetilde{q}_0$, equating the values of a_2 for $\widetilde{q}_0$ and $\widetilde{q}_3$. We also take[2] $2\widetilde{s}/(\widetilde{\bar{u}} + \widetilde{\bar{d}}) = 1/2$. Although these assumptions seem overly restrictive, the quality of the data does not allow us to fit many of these parameters. We discuss some of these points later in this paper.

[2]This is our only assumption about the flavour decomposition of the polarised sea quarks.

The main difference between our parametrisation and previous ones is that we explicitly include a non-zero $\widetilde{q}_3(x,Q_0^2)$ and break $SU(2)$ flavour symmetry in the polarised sea. This part of the sea density is actually quite well constrained, and plays a crucial role in our fits.

2.3 The Bjorken sum rule

The polarised densities are constrained by the Bjorken sum rule. At NLO this reads—

$$\Gamma_1^p(Q^2) - \Gamma_1^n(Q^2) \;=\; \frac{g_3}{6}\left\{1 - \frac{\alpha_S}{\pi} + \left(\frac{\alpha_S}{\pi}\right)^2\left[\frac{N_f}{3} - \frac{55}{12}\right]\right\}, \tag{12}$$

where $g_A = -1.2670 \pm 0.0035 = -g_3$ [13] is the neutron beta-decay constant. Using eq. (6), the left hand side of this expression can be expressed as

$$\Gamma_1^p(Q^2) - \Gamma_1^n(Q^2) = \frac{1}{6}\left(1 + \frac{\alpha_S}{2\pi}\widetilde{\mathcal{C}}_q^{(1)}\right)\left[\Gamma_V^3(Q^2) + \Gamma_3(Q^2)\right]. \tag{13}$$

Here $\widetilde{\mathcal{C}}_q^{(1)}$ is the first moment of the NLO quark coefficient function in the g_1 structure function. It is scheme dependent, and in the $\overline{\rm MS}$ scheme it is given by

$$\widetilde{\mathcal{C}}_q^{(1)} = \int_0^1 dx \widetilde{\mathcal{C}}_q(x) = -2. \tag{14}$$

Finally, keeping only terms up to order α_s^2, the Bjorken sum rule can be written as—

$$\Gamma_V^3(Q^2) + \Gamma_3(Q^2) = g_3\left\{1 + \left(\frac{\alpha_S}{\pi}\right)^2\left[\frac{N_f}{3} - \frac{55}{12}\right]\right\}. \tag{15}$$

We use this to constrain the parameter a_0 in $\widetilde{q}_3$ in terms of the remaining free parameters.

2.4 Other sum rules

In a three flavour world, we can write down the following putative sum rule in NLO QCD for the first moments of the nucleon structure functions—

$$\begin{aligned}\frac{5}{2}\Gamma_V^0 \pm \frac{3}{2}(\Gamma_V^3 + \Gamma_3) + \frac{1}{2}\Gamma_8 + 2\Gamma_0 = \left(\pm\frac{3}{2}g_3 + \frac{1}{2}g_8\right)\left\{1 - 3.5833\left(\frac{\alpha_S}{\pi}\right)^2\right\} \\ +2g_0\left\{1 - 1.0959\left(\frac{\alpha_S}{\pi}\right)^2\right\}.\end{aligned} \tag{16}$$

The upper and lower signs belong to protons and neutrons, respectively. In this expression all terms of order α_s^3 or higher have been neglected, and the numerical coefficients are written for $N_f = 3$, since we plan to use this equation at $Q_0^2 = 2.56$ just below the charm threshold. The quantities g_3, g_8 and g_0 are baryonic axial couplings. They are defined as matrix elements of axial vector currents between baryon states. Due to the axial anomaly, the singlet axial-vector current is not conserved. As a result, g_0 picks up a Q^2 dependence [14]. Hence, g_0, the moments, and α_s have to be evaluated at the same Q^2 in eq. (16).

It is not easy to extract g_0 from low-energy hadron data, although there have been some attempts to do this using elastic νp scattering [15]. This gives $g_0 = 0.14 \pm 0.27$. Lattice computations [16] and QCD sum rules [17] also give similar numbers, but have systematic uncertainties which have to be removed in future. We have already mentioned that g_3 is obtained from neutron beta-decay. The coupling g_8 is extracted from the decay of strange to non-strange baryons. $SU(3)$ flavour symmetry is used crucially in this extraction [18]. The PDG result is $g_8 = 0.579 \pm 0.025$ [13].

The only sum-rule that one can obtain from eq. (16) is the Bjorken sum rule (eq. 15). The Ellis-Jaffe sum rule corresponds to the choice $g_8 = g_0$, and cannot be correct in QCD because g_0 is Q^2 dependent and g_8 is not. Moreover, in the absence of a real measurement of $g_0(Q^2)$, no other sum rule can be extracted from eq. (16). Hence, we use this equation to extract g_0 rather than to impose it as a constraint on parton densities.

2.5 Positivity

Polarisation asymmetries are the ratios of the difference and sum of physically measurable cross sections. Since cross sections are non-negative, asymmetries are bounded by unity in absolute value. In the parton model or in LO QCD, these cross sections are directly related to parton densities. Hence positivity of cross sections imply

$$\left| \frac{\widetilde{f}(x, Q^2)}{f(x, Q^2)} \right| \leq 1 \tag{17}$$

for the ratio of each polarised and unpolarised density to leading order in QCD. In our LO fits, we impose these restrictions.

However, at NLO and beyond, this simple relation between parton densities and cross sections no longer holds. Parton densities are renormalisation scheme dependent object; although universal, they are not physical. Hence there are corrections to positivity [19]. We do not impose eq. (17) on our NLO fits. Nevertheless, we find that the NLO best fit does satisfy this constraint for all the densities.

2.6 Choice of numerical techniques

Our numerical goal is to evolve parton density functions with absolute errors of at most 10^{-3}. If this design goal were reached, then numerical errors would lie at least an order of magnitude below all other errors. We integrate the evolution equations using a 4-th order Runge-Kutta algorithm. The Mellin convolutions required in the evaluation of the derivative are computed using a Gauss-Legendre integral. The parton densities are evaluated on a grid and interpolated using a cubic spline method. All the numerical algorithms may be found in [20].

The knot points of the cubic spline are selected to give an accuracy of 10^{-5} in the evaluation of the parton densities. The Mellin convolutions are also accurate to this order. We require the Runge-Kutta to give us integration errors bounded by 10^{-4}. This gives us the error limits we require. We can test these estimates by checking that all sum rules are satisfied to within 10^{-3}. On a 180 MHz R10000 processor, the program takes about 0.15 CPU seconds to evolve the parton densities by $\Delta Q^2 = 1$ GeV^2.

3 Selection of data

3.1 Data

Experiments do not measure the asymmetry A_1 directly; they measure the asymmetry between the cross sections for lepton and longitudinally polarised protons being parallel and anti-parallel—

$$A_L = \frac{d\sigma(\uparrow\uparrow) - d\sigma(\uparrow\downarrow)}{d\sigma(\uparrow\uparrow) + d\sigma(\uparrow\downarrow)}, \tag{18}$$

or a similar asymmetry, A_T, with transversely polarised protons. These asymmetries are related to the two that we require by

$$A_L = D(A_1 + \eta A_2) \qquad \text{and} \qquad A_T = d(A_2 - \xi A_1), \tag{19}$$

where D and d are depolarisation factors for the virtual photon and ξ and η are essentially kinematic constants. In terms of the ratio of the Compton scattering cross sections for transversely and longitudinally polarised virtual photons,

$$R = \frac{\sigma_{_L}}{\sigma_{_T}} = \frac{F_2 - 2xF_1}{2xF_1}, \tag{20}$$

we can write

$$D = \frac{y(2-y)}{y^2 + 2(1-y)(1+R)}, \qquad \text{and} \qquad \eta = 2\gamma\frac{1-y}{2-y}. \tag{21}$$

Here $\gamma = 2Mx/Q \ll 1$. Using the degree of transverse polarisation of the virtual photon,

$$\epsilon = \frac{1-y}{1-y+y^2/2}, \tag{22}$$

we can write

$$d = D\sqrt{\frac{2\epsilon}{1+\epsilon}}, \qquad \text{and} \qquad \xi = \eta\frac{1+\epsilon}{2\epsilon}. \tag{23}$$

Since γ is very small in the DIS region, the relations $A_L = DA_1$ and $A_T = dA_2$ are actually satisfied to high accuracy. We then use the further relations

$$A_1 = (g_1 - \gamma^2 g_2)/F_1 \qquad \text{and} \qquad A_2 = \gamma(g_1 + g_2)/F_1, \tag{24}$$

to obtain eq. (1) when $\gamma \ll 1$. It is clear from the second equation that g_2 is difficult to measure.

The main theoretical uncertainty in measurements of A_1 is in the values of R used. In fact, many experiments use R in two ways. First, it enters the expression for D and d, and hence is used to construct A_1 and A_2 from A_L and A_T. Next, it is used along with measurements of F_2 to compute F_1 and thus relate g_1 to A_1. We bypass this second use of R by utilising experimental data on A_1 instead of g_1. We are forced, however, to accept the first use of R, In any case, differences between experiments in their estimates of D should be factored into the overall normalisation errors.

The SMC collaboration has data from muon scattering off both proton and deuterium targets. Data was taken in separate runs in 1993 and 1996. The most recent publication for A_1 is [21]; this supersedes previously published data. The E-143 experiment at SLAC has data from electron scattering off proton, deuterium and ^3He targets. Their most recent publication is [22], which supersedes all previous published data on $A_1(x, Q^2)$ by this collaboration. The E-154 experiment at SLAC has data from electron scattering off ^3He targets [23]. The HERMES collaboration in DESY has data from positron scattering off protons and ^3He [24]. We have also used data on DIS from ^3He taken by the SLAC E-142 collaboration [25]. We have chosen not to utilise data taken by the older EMC collaboration and the E-140 experiments at SLAC.

Deuterium is a spin-1 nucleus with the p and n primarily in a relative s-wave state. The d-wave probability is estimated to be $\omega_D = 0.05 \pm 0.01$ [26]. This is used in the relation between the structure function of deuterium and those of p and n— $g_1^d = (1-3\omega_D/2)(g_1^p + g_1^n)/2$. In ^3He, the two protons are essentially paired into a spin singlet, and the asymmetry is largely due to the unpaired neutron. Corrections due to other components of the nuclear wave-function are small [27]. More details are available in [28].

From the chosen experiments, we have retained only the data on $A_1(x, Q^2)$ for $Q^2 \geq 2.56$ GeV^2. While this does remove some of the low-x data, the error bars in the removed data are pretty large. We have checked by backward evolution that the data which is removed would not have constrained the fits any further. The total number of data points used in our analysis is 224.

In most fitting procedures the statistical errors on measurements are combined in some way with the systematic error estimates. Both sets of errors are usually reported in the literature in each bin of data. Whereas this procedure is acceptable for statistical errors, it oversimplifies the nature of systematic errors. These latter are correlated from bin to bin, and one must use the full covariance matrix of errors in the analysis. In the absence of published information on the covariance matrix, one may make the simplifying assumption that the bin-to-bin correlation vanishes, and add the statistical and systematic errors in quadrature. This overestimates the errors on data and hence the errors on the parameters determined by fitting. We have made a different extremal assumption of neglecting the systematic errors altogether. This procedure almost certainly makes us under-estimate the parameter errors— a point to be borne in mind when we discuss large errors and uncertainties in

the fits. In summary, our choice of error analysis is deliberately conservative.

Since g_2 contains a possible twist-3 contribution, which cannot be written in terms of parton distributions, we cannot utilise data on g_2 for our fits. However, the twist-2 part is completely determined by g_1. In a later section, we report an attempt to limit the extent of the twist-3 term using our fitted polarised parton densities. For this we have utilised data on proton target from SMC and the E-143 collaboration at SLAC [29], on deuterium target from SMC, E-143 and SLAC E-155 [30], and on neutron target from the E-143 and SLAC experiment E-154 [31]. In all cases, we have used the most recent data set and analysis from each collaboration. The quality of data on g_2 is poorer than that for g_1. This is because A_2 is small, and extraction of g_2 from A_2 requires the subtraction of g_1, which itself has significant measurement errors. The errors are dominated by statistical uncertainties.

There remains data from semi-inclusive DIS taken by the SMC [32] and HERMES [33] experiments. Analysis of these require polarised fragmentation functions and their Q^2 evolution. Since the data on fragmentation is very rudimentary, we have not utilised this data in our fits.

4 Results

Polarised parton densities obtained from the global fit to data in next-to-leading order QCD are summarised in Table 1. Errors in $\widetilde{V}_u$ and $\widetilde{V}_d$ are small. The normalisation of $\widetilde{q}_3$ inherits its error from g_3 and the other valence parameters. Apart from this, the sea densities are almost unconstrained. The gluon densities, surprisingly, seem to be constrained better. The quality of the fit is shown in Figures 1–3. It is useful to note that the positivity conditions are satisfied by these densities, although they were not imposed while fitting. We recommend that these parametrisations be used with the CTEQ4M set of unpolarised parton densities [8]. For this set $\Lambda^{(5)} = 0.202$ GeV.

In Fig 4 we have plotted

$$\Delta\chi^2 = \chi^2 - \chi^2_{\rm min} \tag{25}$$

against the parameter a_1 for $\widetilde{q}_0$, for fixed values of the other parameters. Usually the minimum of such a curve fixes the value of the parameter, and the points where $\Delta\chi^2 = 1$ give the 68.3% confidence limits on the parameter.

density	a_0	$1+a_1$	a_2	a_3	a_4
$\widetilde{V}_u$	0.57 ($\pm$1)	0.88 ($\pm$2)	3.689^b	14.1 ($\pm$2)	0.873^b
$\widetilde{V}_d$	-0.49 ($\pm$1)	0.88^a	4.247^b	2.7 ($\pm$2)	0.333^b
$\widetilde{q}_0$	-0.02 ($\pm$2)	> 1.4	8.041^b	6.112^b	1.000^b
$\widetilde{q}_3$	0.05 ($\pm$1)	0.88^a	8.041^b	0.^{b}	30^b
$\widetilde{g}$	-2 ($\pm$1)	1.0 ($^{+4}_{-2}$)	4.673^b	-6 ($\pm$2)	1.508^b

Table 1: The NLO fits for the parameters in eqs. (10, 11) at $Q_0^2 = 2.56$ GeV^2. The error estimates shown in the brackets apply to the last digit of the estimated value. The fit gives $\chi^2 = 241$ for 215 DOF. The parameters marked (a) are set equal to some other in the same column, and (b) are fixed to the value taken by the unpolarised densities.

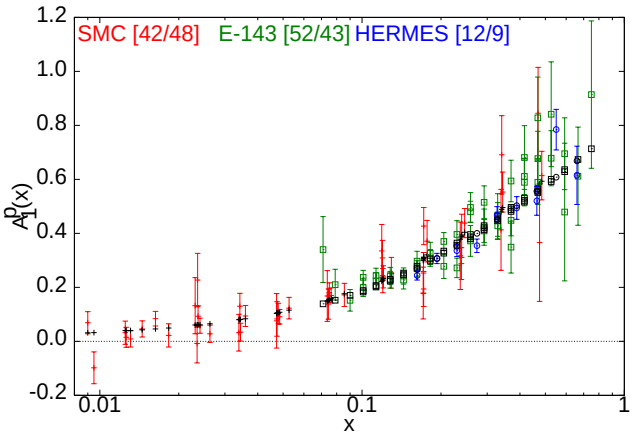

Figure 1: Data and fits for A_1^p. The coloured points show data. The fits, shown in black, give A_1^p at the x and Q^2 values for the corresponding data. The numbers in brackets show the values of χ^2/DOF.

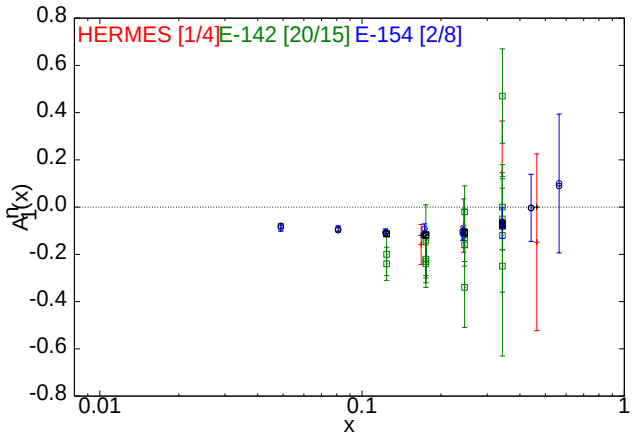

Figure 2: Data and fits for A_1^n. The coloured points show data. The fits, shown in black, give A_1^n at the x and Q^2 values for the corresponding data. The numbers in brackets show the values of χ^2/DOF.

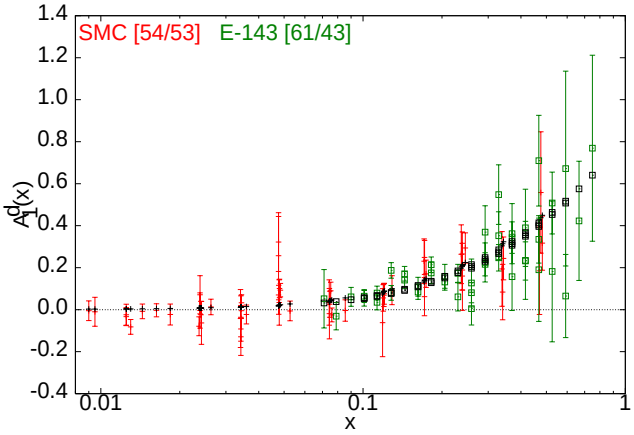

Figure 3: Data and fits for A_1^d. The coloured points show data. The fits, shown in black, give A_1^d at the x and Q^2 values for the corresponding data. The numbers in brackets show the values of χ^2/DOF.

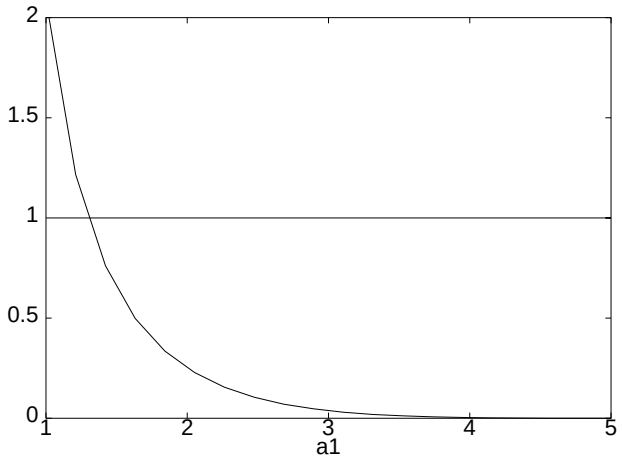

Figure 4: Plot of $\Delta\chi^2$ against the parameter a_1 for the polarised sea quark density $\widetilde{q}_0$. This puts only a lower limit on the parameter.

This case, however, looks pathological, since the curve is flat on one side— it cuts the $\Delta\chi^2 = 1$ line only in one point. This point can then be interpreted as the 68.3% confidence (lower) limit on the parameter. Any higher value of a_1 can be used with the rest of these parametrisations.

This behaviour of the polarised sea quark density is easily understood. The asymmetry is nearly saturated by the polarised valence quark density. The only window of visibility of the polarised sea densities is at low-x where the asymmetry is vanishing and the measurement errors are large. At small x, since $\widetilde{q}_0 \sim x^{a_1}$, the lower limit on a_1 only tells us that the sea quark density has to be small enough.

We also investigated freezing and unfreezing the remaining parameters in the sea quark density. It turns out that they are very ill-determined. For example, the parameters a_3 for $\widetilde{q}_0$ and a_4 for $\widetilde{q}_3$ have errors of a few hundred percent. In view of this, we have kept the parameters frozen at their unpolarised values.

Figure 5 shows plots of $\Delta\chi^2$ against the gluon density parameters a_0, a_1 and a_3. The pathological behaviour seen in the sea quark densities is absent. Parameter errors are symmetric except for those in a_1. The correlation between the two parameters a_0 and a_1 for the polarised gluon distribution is

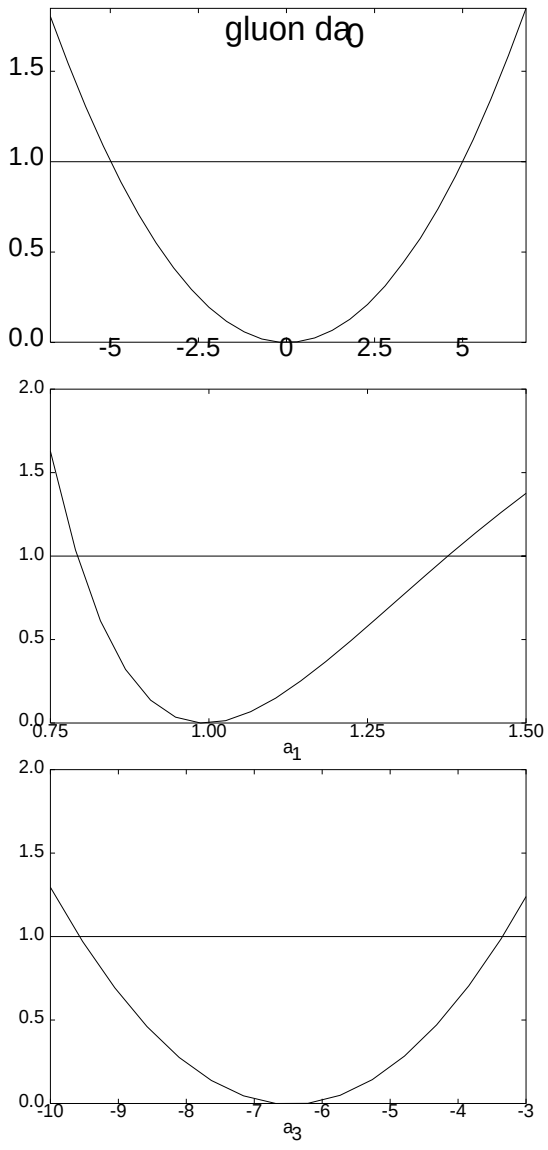

Figure 5: Plots of $\Delta\chi^2$ against the parameter a_0, a_1 and a_3 for the polarised gluon density $\widetilde{g}$.

shown in Figure 6. The contour line with $\Delta\chi^2 = 2.3$ encloses the area with 68.3% probability of giving a good description of the data. Also shown in the figure are lines of constant $\Gamma_g(Q_0^2)$. It seems that the 1σ contour roughly encloses the area with $-1 \leq \Gamma_g \leq -0.02$. These parameter errors translate into huge uncertainties in the gluon distribution. In Figure 7 we have shown the two polarised valence quark densities along with the regions of uncertainty in the gluon distribution. At $x = 0.01$ the polarised gluon density can lie anywhere in the range from -50 to 1. This uncertainty at low-x prevents us from investigating this theoretically interesting region.

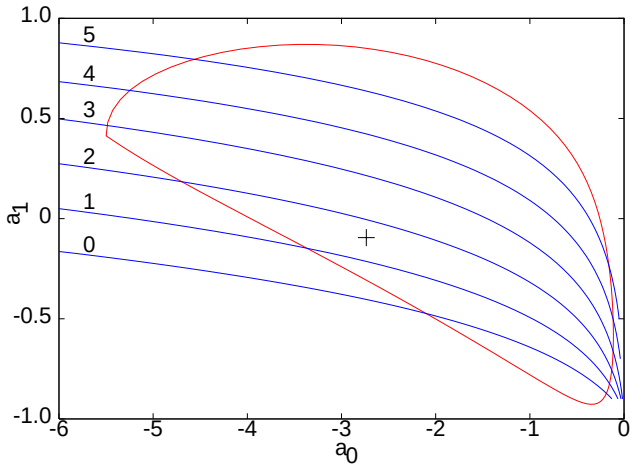

Figure 6: The covariance of the fitted parameters a_0 and a_1 for the polarised gluon density $\widetilde{g}$. The cross shows the best fit point, and red line is the contour of $\Delta\chi^2 = 2.3$. Along the blue lines $\Gamma_g = -1/2^n$, for the values of n marked.

The influence of these variations on g_1^p is shown in Figure 8. The variation due to the gluon densities is largest at the lowest values of x, where the only data is from the old SMC experiment. This data set is not able to constrain the gluon density well. In order to do a better job with DIS experiments, the measurement errors on A_1^p have to be brought down to the level of the uncertainty band at $x \approx 0.05$. This means that at these values of x the errors have to be of the order of the measurement errors in the HERMES experiment at $x \approx 0.25$.

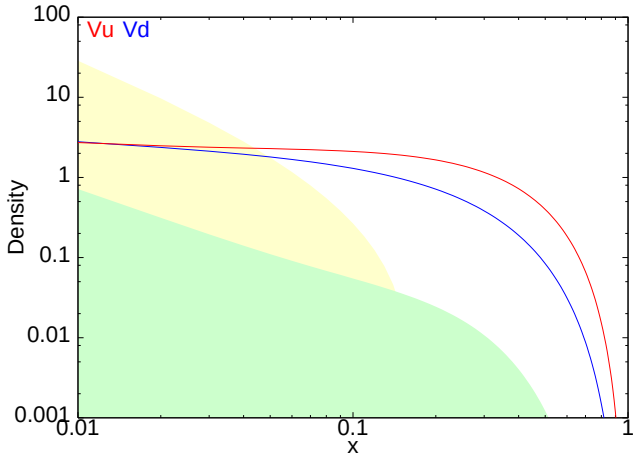

Figure 7: The absolute values of the polarised valence quark densities are shown along with the uncertainties in the polarised gluon density. The patch in green shows the uncertainty for those parameter values which lead to a positive value of $\widetilde{g}$, and the patch in yellow does the same for negative $\widetilde{g}$.

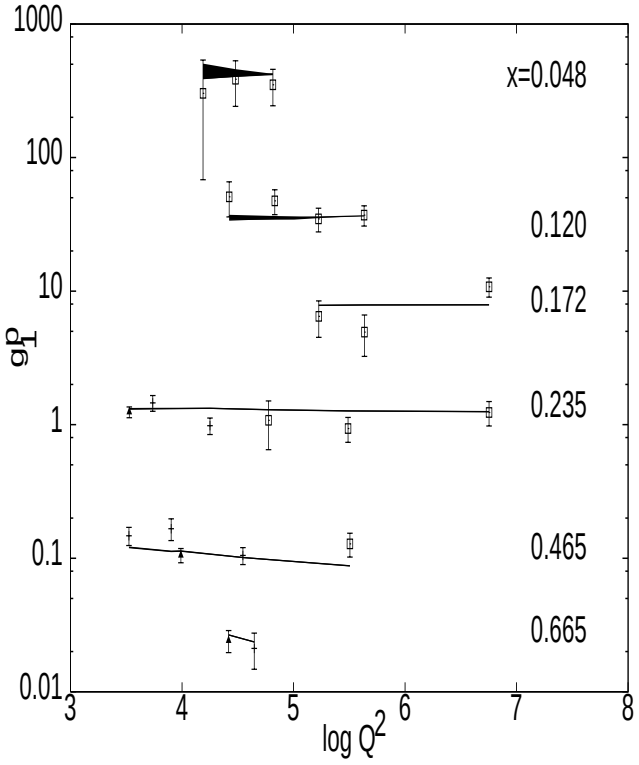

Figure 8: Plot of $g_1^p(x, Q^2)$ in different bins of x as a function of $\log(Q^2/\Lambda^2)$. The bands are the uncertainty in the NLO QCD prediction due to the uncertainty in the gluon distribution parameters. The SMC measurements are indicated by boxes, E-143 by pluses and HERMES by triangles. Data in different bins of x are offset for visibility.

In order to investigate the accuracy to which gluon and sea quarks could be determined by decreasing errors in measurement of g_1 in the low-x region we have generated fake data from our NLO fits for $0.09 < x < 0.125$. We replaced all data on A_1 in this range by this faked data set to which we assigned 25% statistical error. For the parameters a_0 and a_1 of $\tilde{g}$ and $\tilde{q}_0$, plots of $\Delta\chi^2$ against the deviation from the best value are shown in Figure 9. It is seen that the gluon and singlet sea quark parameters can be fixed with 3 figure accuracy (1–0.1%) if measurement errors in g_1 can be brought down to this level. It seems that the polarised option at HERA can perform such a measurement [34]. Good statistics are also expected at the proposed 100 GeV or 200 GeV muon beam polarised option at the fixed target experiment, COMPASS, already under construction at the CERN SPS [35].

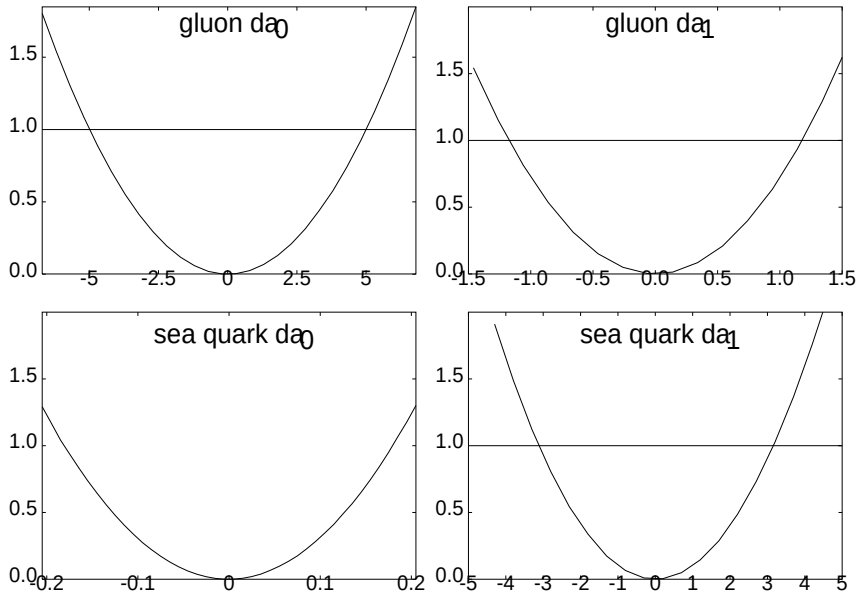

Figure 9: Plot of $\Delta\chi^2$ against the deviation from the central value of the gluon and singlet sea quark parameters a_0 and a_1 using faked data with 25% errors in measurements of A_1 for $x < 0.125$. The units on the x-axis are 10^{-3}.

For completeness we show the parton density set obtained from a leading

order QCD fit in Table 2. We recommend that this parameter set be used with the CTEQ4L set of parametrisations for unpolarised parton densities. Errors in $\widetilde{V}_u$ and $\widetilde{V}_d$ are small. The singlet sea density is fixed better at LO. This is due to the fact that g_1 has no gluon contribution, and hence the fit to the sea density is not destabilised by the errors in the gluon density. On the other hand, since the gluon does not enter into g_1 through a coefficient function, it is much less well-determined at LO.

density	a_0	$1+a_1$	a_2	a_3	a_4
$\widetilde{V}_u$	1.566^{+5}_{-0}	0.842^{+0}_{-1}	3.465^b	4.28^{+5}_{-0}	1.146^b
$\widetilde{V}_d$	-0.70^{+0}_{-2}	0.842^a	4.003^b	1.7^{+1}_{-0}	0.622^b
$\widetilde{q}_0$	-0.05 ($\pm$3)	1.8 ($\pm$3)	6.877^b	3 ($\pm$6)	1.000^b
$\widetilde{q}_3$	-0.09 ($\pm$1)	0.842^a	6.877^b	$0.^b$	33 ($\pm$8)
$\widetilde{g}$	0.0 ($\pm$2)	1 ($\pm$1)	3.666^b	26 ($\pm$10)	1.968^b

Table 2: The LO fits for the parameters in eqs. (10, 11) at $Q_0^2 = 2.56$ GeV^2. Many errors are asymmetric, with the parameters being at the limit of positivity (this is indicated by one of the errors being zero). The fit gives $\chi^2 = 281$ for 213 DOF. The superscripts on the numbers have the same meaning as in Table 1.

5 Applications

5.1 Flavour asymmetry

Unlike previous fits of parton densities which had built in the constraint $\widetilde{\bar{d}} \approx \widetilde{\bar{u}}$ [7], we have allowed for sea quark densities that violate flavour $SU(2)$ symmetry. The fits show that the data tolerate strong flavour symmetry violations. This is easily seen in the first moments of various densities (Table

Moment	NLO	LO
Γ_u	0.59 (4)	0.784 (3)
Γ_d	-0.28 (2)	0.298 (7)
Γ_0	0.	-0.002 (1)
Γ_g	-0.2^{+2}_{-8}	0. (1)
Γ_3	0.34	0.079
$2\Gamma_{\bar{u}}$	0.17	0.039
$2\Gamma_{\bar{d}}$	-0.17	-0.040
$2\Gamma_{\bar{s}}$	0.	0.

Table 3: Moments of various densities at $Q_0^2 = 2.56$ GeV^2. By our initial conditions $\Gamma_8 = 2\Gamma_0/5$. When errors are not shown, they can be obtained from those of the others.

3). Since Γ_3 is large, and Γ_0 and Γ_8 are almost vanishing, it is clear that the pattern $\Gamma_s \approx 0$ and $\Gamma_{\bar{d}} \approx -\Gamma_{\bar{u}}$, seen in the table must follow. This flavour antisymmetry is very easy to test at the RHIC through measurements of spin asymmetries in $W^{\pm}$ production. In the two cases, $\widetilde{\bar{d}} = \pm\widetilde{\bar{u}}$, the spin asymmetries for W^+ production will have opposite sign.

We also find that our NLO fits yield a negative first moment for the gluon density. Although previous fits have seen overlapping ranges of allowed Γ_g, the theoretical bias has been to take large and positive values of Γ_g. The LO fit is unable to decide on the sign of this quantity. This sign can be easily fixed by various experiments at RHIC or in charm production measurements at HERA [34] or the COMPASS experiment in CERN [35].

We would like to caution that parton densities are renormalisation scheme dependent (and hence unphysical). They are universally applicable to all experiments, as long as each experiment is treated in the same scheme [36]. Our determination of these densities are in the $\overline{\rm MS}$ scheme, and statements about their moments are therefore also restricted to this scheme. When interpreting the moments of unphysical parton densities, their scheme dependence must be held in mind.

5.2 Structure functions and couplings

It is possible to construct physical quantities out of the unphysical first moments of the parton densities. For the first moments of the structure functions, we obtain, using the NLO expressions which give rise to eqs. (15,16), the values—

$$\Gamma_1^p = 0.129 \pm 0.004 \qquad \text{and} \qquad \Gamma_1^n = -0.052 \pm 0.003, \tag{26}$$

at $Q_0^2 = 2.56$ GeV^2. These values compare well with those deduced from experiments [1, 23, 25]. We can also use eq. (16) to extract the value of g_0. Using as input our fits and the PDG value for g_8, we find

$$g_0(Q_0^2) = 0.14 \pm 0.05. \tag{27}$$

Since g_0 is a physical quantity, it is only to be expected that our determination of g_0 should agree with other analyses, such as [9], even if they use some other scheme to arrive at the same result. We will, of course, disagree with them on any scheme dependent quantity, such as $\Delta\Sigma = \Gamma_u + \Gamma_v + \Gamma_0$. Our maximally flavour symmetry violating fits give physically reasonable results.

5.3 The structure function g_2

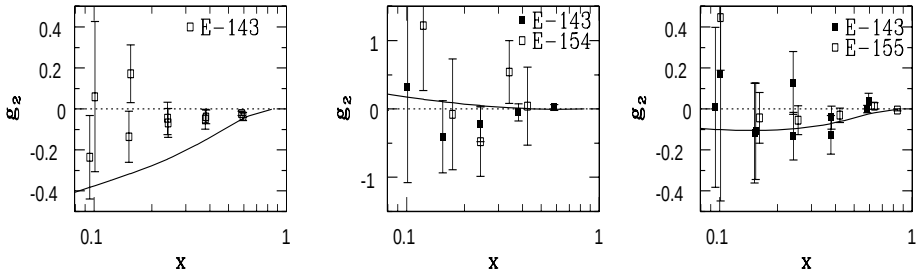

Figure 10: Data on the structure function g_2 compared with the twist-2 predictions of eq. (28) evaluated with our NLO parametrisation evolved to $Q^2 = 5$ GeV^2. From left to right, the figures are for g_2^p, g_2^n and g_2^d.

Wandzura and Wilczek [37] have derived a sum rule relating the twist-2 part of g_2 to g_1—

$$g_2^{WW}(x, Q^2) = -g_1(x, Q^2) + \int_x^1 \frac{g_1(y, Q^2)}{y} \mathrm{d}y. \tag{28}$$

An additional twist-2 contribution to g_2, suppressed by the ratio of the quark to the nucleon mass [38], is ignored here. Predictions for the twist-3 contribution have been made using bag models [39], QCD sum rules [40] as well as from non-perturbative lattice QCD computations [41]. Since some computations predict large twist-3 contributions to moments of g_2, it becomes interesting to check whether the data on g_2 allows such contributions.

Figure 10 shows our "prediction" for the twist-2 part of g_2 and compares it to measurements of this structure function. Clearly the data is compatible with the NLO twist-2 prediction (and also with the parton model result, $g_2 = 0$). Between the prediction and the data, there is little room for a twist-3 contribution. Statistics have to be improved vastly in order to study higher-twist effects. In fact, COMPASS hopes to make this measurement [35].

Since the statistical errors are smallest for g_2^d, it seems that this is the best candidate in which to look for twist-3 effects. However the data quality needs

improvement even here. There is considerable scaling violation in the twist-2 part of g_2, but the large errors prevent any analysis of the Q^2-dependence.

5.4 The valence densities

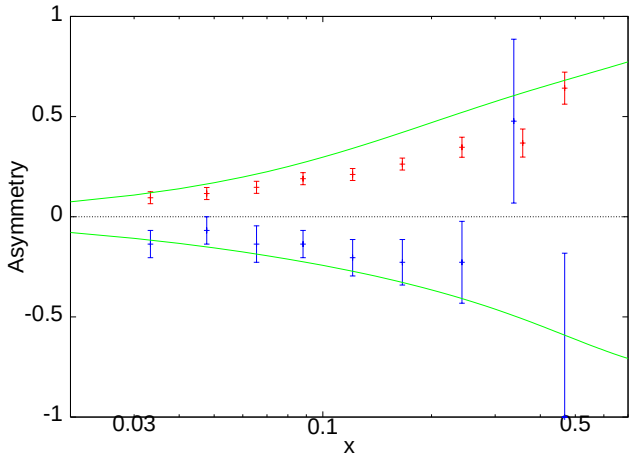

Figure 11: The asymmetries $(\widetilde{u}+\widetilde{\bar{u}})/(u+\bar{u})$ (in red) and $(\widetilde{d}+\widetilde{\bar{d}})/(d+\bar{d})$ (in blue) extracted by a parton model analysis of experimental data [33] (the two overlapping points at $x = 0.35$ have been separated for clarity) compared to our NLO fits at $Q^2 = 25$ GeV^2.

Recently the HERMES collaboration has used semi-inclusive polarised DIS data to extract valence and sea quark densities [33]. We have not used these in our fits because this analysis is performed with parton model formalæ. Nevertheless, it is interesting to compare our fits with these numbers. We display this comparison in Figure 11. The rough agreement is heartening, but the small systematic differences between the fit results and the HERMES extraction of the valence densities shows the need for a more accurate QCD analysis of the experimental data, taking into account properly the Q^2 dependence through NLO evolution.

5.5 Axion-matter coupling

We present an example of the application of polarised proton scattering to physics beyond the standard model. The Peccei-Quinn solution to the strong CP problem postulates a global symmetry whose spontaneous breakdown generates a (nearly) massless pseudo-Goldstone boson called the axion [42]. There is a variant of the original model which is still viable [43]. The axion, a, whose decay constant is f_a, couples to fermions, ψ_f, of mass m_f by the term

$$\mathcal{L}_{int} = -ig_f\,\bar{\psi}_f\gamma_5\psi_f\,a. \tag{29}$$

The coupling $g_f = C_f(m_f/f_a)$. The effective Peccei-Quinn charge, $C_f = X_f/N$, appears in the coupling instead of the actual charge X_f. Here, N is given by $\sum X_f$. There have been several studies [44] of the effective Peccei-Quinn charge of the proton. For three flavours, the LO expression can be written as

$$\begin{aligned} C_p &= (C_u-\mu_u)\Gamma_u + (C_d-\mu_d)\Gamma_d + \frac{1}{2}\left[(C_u-C_d)-(\mu_u-\mu_d)\right]\Gamma_3 \\ &\quad + \frac{2}{5}\left[(C_u+C_d+\eta C_s)-(\mu_u+\mu_d+\eta\mu_s)\right]\Gamma_0, \end{aligned} \tag{30}$$

where $\mu_f = M/m_f$ and $1/M = \sum 1/m_f$ [45]. In our parametrisation $\eta = 1/2$. C_n is obtained from C_p by an isospin flip of the moments. The effective Peccei-Quinn charge for quarks and leptons is highly model dependent. In the so-called KSVZ [46], and other hadronic axion models, $C_u = C_d = C_s = 0$. Using quark mass ratios $m_u/m_d = 0.568 \pm 0.042$ and $m_u/m_s = 0.0290 \pm 0.0043$, obtained by chiral perturbation theory [47], and our LO fits, we find that

$$C_p = -0.39 \qquad \text{and} \qquad C_n = -0.08. \tag{31}$$

Each of these couplings has an error of about 20%, which comes from a combination of the errors in our fit and the errors in the quark mass ratios. Using our LO fits, the difference $C_p - C_n$ is dominated by Γ_V^3.

The chiral couplings of neutralinos and charginos in generic supersymmetric extensions of the standard model also give rise to effective couplings with matter which depend on the moments of the parton densities. Such couplings are often needed in astrophysical contexts. Unless these couplings

are examined to 2-loop order, they should not be evaluated with the NLO moments.

6 Conclusions

We have made a global QCD analysis of data on the asymmetry A_1 from polarised DIS without making overly restrictive assumptions about the flavour content of the sea. We have extracted sets of polarised parton densities which can be used with the CTEQ4 set of unpolarised densities. Our NLO analysis (in the $\overline{\rm MS}$ scheme) yields the parameter set given in Table 1, and the LO analysis gives the set displayed in Table 2. We found that the gluon densities are not very well constrained by data. Furthermore, in our NLO analysis, the singlet sea quark density is extremely badly determined. However, its first moment is very close to zero, whereas that of the triplet sea quark density is not. This implies strong $SU(2)$ flavour symmetry violation in the sea. We also found in the NLO fit that the first moment of the gluon density is preferentially negative. The LO fit cannot decide the sign of this moment. All physical quantities obtained from the first moments of our fitted densities have completely sensible values.

$SU(2)$ flavour symmetry violation in the polarised sea densities can be easily tested by observing polarisation asymmetries for $W^{\pm}$ produced at RHIC. The sign of the W^+ asymmetry depends on whether the sea is $SU(2)$ symmetric or antisymmetric. The moment of the gluon density can be checked either at RHIC or in charm production at HERA or the COMPASS experiment at CERN.

We have shown that the polarised HERA option may give better than 1% accuracy in measurements of the polarised sea and gluon densities if measurements of A_1 in the range $x \leq 0.125$ can be performed with errors of about 25%. Such measurements would nicely complement the possible constraints from RHIC.

We have checked that our parametrisations are roughly consistent with semi-inclusive DIS data, although a full QCD analysis of this data remains to be performed. We have shown that these parametrisations, when used to determine the twist-2 part of g_2 leave very little room for a twist-3 part to this structure function. Finally, we have determined the coupling of hadronic axions to matter— an input into several astrophysical constraints on the

invisible axion.

In a future publication we plan to make a more detailed study of several issues, including the proper inclusion of systematic experimental errors into the analysis and several other technical issues concerning NLO QCD global fits. We also plan to explore flavour symmetry and its breaking in detail.

We would like to thank Willy van Neerven for several discussions and clarifications. We would also like to thank the organisers of the 6th Workshop on High Energy Physics Phenomenology (WHEPP-6), Chennai, January 2000, where a portion of this work was completed.

References

[1] M. J. Alguard *et al.* (E80), *Phys. Rev. Lett.* 37 (1976) 1261;
G. Baum *et al.* (E130), *Phys. Rev. Lett.* 51 (1983) 1135;
J. Ashman *et al.* (EMC), *Phys. Lett.* B 206 (1988) 364.

[2] J. Ellis and R. Jaffe, *Phys. Rev.*, D 9 (1974) 1444; Erratum— *ibid.*, D 10 (1974) 1669;
M. Gourdin, *Nucl. Phys.*, B 38 (1972) 418.

[3] J. D. Bjorken, *Phys. Rev.*, 148 (1966) 1467,

[4] S. A. Larin and J. A. M. Vermaseeren, *Phys. Lett.*, B 259 (1991) 345.

[5] G. Altarelli *et al.*, *Nucl. Phys.*, B 496 (1997) 337.

[6] R. Mertig and W. van Neerven, *Z. Phys.*, C 70 (1996) 637;
W. Vogelsang, *Phys. Rev.*, D 54 (1996) 2023.

[7] M. Glück *et al.*, *Phys. Rev.* D 53 (1996) 4775;
T. Gehrmann and W. J. Stirling, *Phys. Rev.*, D 53 (1996) 6100;
K. Abe *et al.* (E-154), *Phys. Lett.* B 405 (1997) 180;
C. Bourrely *et al.*, *Prog. Theor. Phys.* 99 (1998) 1017;
G. Altarelli *et al.*, *Acta Phys. Polon.* B 29 (1998) 145;
D. de Florian, O. Sampayo and R. Sassot, *Phys. Rev.*, D 57 (1998) 5803;
L. E. Gordon, M. Goshtasbpour and G. P. Ramsey, *Phys. Rev.* D 58 (1998) 094017;
E. Leader, A. V. Sidorov and D. B. Stamenov, *Phys. Rev.* D 58 (1998) 114028;
Y. Goto *et al.*, e-print hep-ph/0001046.

[8] H. L. Lai *et al.*, *Phys. Rev.*, D 55 (1997) 1280.

[9] R. D. Ball, S. Forte and G. Ridolfi, *Phys. Lett.* B 378 (1996) 255.

[10] E. Leader, A. V. Sidorov and D. B. Stamenov, *Phys. Lett.* B 445 (1998) 232.

[11] W. J. Marciano, *Phys. Rev.*, D 29 (1984) 580;
J. F. Owens and W.-K. Tung, *Ann. Rev. Nucl. Part. Sci.*, 42 (1992) 291.

[12] F. E. Close and D. Sivers, *Phys. Rev. Lett.* 39 (1977) 1116;
S. J. Brodsky and I. Schmidt, *Phys. Lett.* B 234 (1990) 114.

[13] C. Caso *et al.*, *Euro. Phys. J.* C 3 (1998) 1;
The Particle Data Group, http://pdg.lbl.gov, June 1999.

[14] R. L. Jaffe, *Phys. Lett.*, B 193 (1987) 101.

[15] L. H. Ahrens *et al.*, *Phys. Rev.* D 35 (1987) 785.

[16] M. Fukugita *et al. Phys. Rev. Lett.* 75 (1995) 2092;
S. J. Dong *et al. Phys. Rev. Lett.* 75 (1995) 2096.

[17] S. Gupta, M. V. N. Murthy and J. Pasupathy, *Phys. Rev.* D 39 (1989) 2547;
E. M. Henley, W. Y. P. Hwang and L. S. Kisslinger, *Phys. Rev.* D 46 (1992) 431.

[18] D. B. Kaplan and A. Manohar, *Nucl. Phys.* B 310 (1988) 527;
H. J. Lipkin, *Phys. Lett.* B 230 (1988) 135;
M. Anselmino, B. L. Ioffe and E. Leader, *Sov. J. Nucl. Phys.* 49 (1989) 136;
E. Leader and D. B. Stamenov, e-print hep-ph/9912345.

[19] G. Altarelli, S. Forte and G. Ridolfi, *Nucl. Phys.*, B 534 (1998) 277.

[20] W. H. Press *et al.*, *Numerical Recipes in Fortran*, Cambridge University Press, 1990.

[21] B. Adeva *et al.* (SMC), *Phys. Rev.* D 58 (1998) 112001.

[22] K. Abe *et al.* (E143), *Phys. Rev.* D 58 (1998) 112003.

[23] K. Abe *et al.* (E154), *Phys. Rev. Lett.* 79 (1997) 26.

[24] A. Airapetian *et al.* (HERMES), *Phys. Lett.* B 442 (1998) 484.

[25] P. L. Anthony *et al.* (E142), *Phys. Rev.* D 54 (1996) 6620.

[26] B. Desplanques, *Phys. Lett* B 203 (1988) 200;
A. W. Thomas and W. Melnitchouk, *Nucl. Phys.* A 631 (1998) 296c.

[27] R. M. Woloshyn, *Nucl. Phys.* A 496 (1988) 749;
S. Scopetta *et al.*, *Phys. Lett.* B 404 (1997) 223.

[28] M. Anselmino, A. Efremov and E. Leader, *Phys. Rep.* 261 (1995) 1;
B. Lampe and E. Reya, e-print hep-ph/9810270.

[29] D. Adams *et al.* (SMC), *Phys. Rev.* D 56 (1997) 5330;
K. Abe *et al.* (E143), *Phys. Rev.* D 58 (1998) 112003.

[30] D. Adams *et al.* (SMC), *Phys. Lett.* B 396 (1997) 338;
K. Abe *et al.* (E143), *Phys. Rev.* D 58 (1998) 112003;
P. L. Anthony *et al.* (E155), *Phys. Lett.* B 463 (1999) 339.

[31] K. Abe *et al.* (E143), *Phys. Rev.* D 58 (1998) 112003
K. Abe *et al.* (E154), *Phys. Lett.* B 404 (1997) 377.

[32] B. Adeva *et al.* (SMC), *Phys. Lett.* B 420 (1998) 180.

[33] K. Ackerstaff *et al.* (HERMES), *Phys. Lett.* B 464 (1999) 123.

[34] T. Gehrmann, e-print hep-ph/9908500;
J. Feltesse and A. Schäfer, Proceedings of the workshop, "Future Physics at HERA", Hamburg, 1995/96, Eds. G. Ingelman, A. De Roeck, and R. Klanner, DESY (Hamburg, 1996).

[35] L. Schmitt (for the Compass Collaboration), Contribution at the International Conference on High Energy Physics, ICHEP, Vancouver, 1998.

[36] A. Manohar, *Phys. Rev. Lett.* 66 (1991) 289.

[37] S. Wandzura and F. Wilczek, *Phys. Lett.* B 72 (1977) 195.

[38] X. Song, *Phys. Rev.* D 54 (1996) 1955.

[39] M. Stratmann, *Z. Phys.* C 60 (1993) 763;
R. L. Jaffe and X. Ji, *Phys. Rev.* D 43 (1991) 724;
see also [38].

[40] I. I. Balitsky, V. M. Braun, and A. V. Kolesnichenko, *Phys. Lett.* B 242 (1990) 245;
E. Stein *et al.*, *Phys. Lett.* B 343 (1995) 369.

[41] M. Göckeler *et al.*, *Phys. Rev.* D 53 (1996) 2317.

[42] R. D. Peccei and H. Quinn, *Phys. Rev. Lett.* 38 (1977) 1440.

[43] M. Dine, W. Fischler and M. Srednicki, *Phys. Lett.* B 104 (1981) 199.

[44] D. B. Kaplan, *Nucl. Phys.* B 260 (1985) 215;
M. Srednicki, *Nucl. Phys.* B 260 (1985) 689;
R. Mele,*et al. Phys. Lett.* B 203 (1988) 188.

[45] G. Raffelt, *Phys. Rep.* 198 (1990) 1.

[46] J. E. Kim, *Phys. Rev. Lett.* 43 (1979) 103;
M. A. Shifman, A. I. Vainshtein and V. I. Zakharov, *Nucl. Phys.* B 166 (1980) 493.

[47] J. Gasser and H. Leutwyler, *Phys. Rep.* 87 (1982) 77.